Talanta 260 (2023) 124614

Contents lists available at ScienceDirect

Talanta

journal homepage: www.elsevier.com/locate/talanta

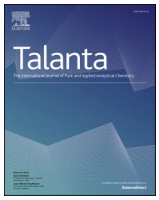

Bifunctional Au@Pt/Au nanoparticles as electrochemiluminescence signaling probes for SARS-CoV-2 detection

Ana M. Villa-Manso [a], Tamara Guerrero-Esteban [a], Félix Pariente [a,b], Celia Toyos-Rodríguez [c,d], Alfredo de la Escosura-Muñiz [c,d], Mónica Revenga-Parra [a,b,*], Cristina Gutiérrez-Sánchez [a,b,**], Encarnación Lorenzo [a,b,e]

[a] Grupo de Sensores Químicos y Biosensores, Departamento de Química Analítica y Análisis Instrumental, Universidad Autónoma de Madrid, 28049, Madrid, Spain
[b] Institute for Advanced Research in Chemical Sciences (IAdChem), Universidad Autónoma de Madrid, 28049, Madrid, Spain
[c] NanoBioAnalysis Group, Departamento de Química Física y Analítica, Universidad de Oviedo, 33006, Oviedo, Spain
[d] Biotechnology Institute of Asturias, Universidad de Oviedo, Edificio Santiago Gascon, 33006, Oviedo, Spain
[e] IMDEA-Nanociencia, Ciudad Universitaria de Cantoblanco, 28049, Madrid, Spain

ARTICLE INFO

Keywords:
COVID-19
SARS-CoV-2
N protein
Immunosensor
Metal nanoparticles
Electrochemiluminescence resonance energy transfer

ABSTRACT

A novel immunosensor based on electrochemiluminescence resonance energy transfer (ECL-RET) for the sensitive determination of N protein of the SARS-CoV-2 coronavirus is described. For this purpose, bifunctional core@shell nanoparticles composed of a Pt-coated Au core and finally decorated with small Au inlays (Au@Pt/Au NPs) have been synthesized to act as ECL acceptor, using $[Ru(bpy)_3]^{2+}$ as ECL donor. These nanoparticles are efficient signaling probes in the immunosensor developed.

The proposed ECL-RET immunosensor has a wide linear response to the concentration of N protein of the SARS-CoV-2 coronavirus with a detection limit of 1.27 pg/mL. Moreover, it has a high stability and shows no response to other proteins related to different virus.

The immunosensor has achieved the quantification of N protein of the SARS-CoV-2 coronavirus in saliva samples. Results are consistent with those provided by a commercial colorimetric ELISA kit. Therefore, the developed immunosensor provides a feasible and reliable tool for early and effective detection of the virus to protect the population.

1. Introduction

The SARS-CoV-2 coronavirus has caused a respiratory syndrome that has had serious consequences not only in terms of human health but also in the global economy. Overcoming this crisis has been and still is a great challenge for today's society that requires a great effort in terms of research at different levels. Due to the rapid spread of the virus and its mode of transmission including droplet, airborne towards microaerosols and direct contact, it has lead infections and deaths in the population. Also, asymptomatic patients with COVID-19, without showing any symptoms, are the main spreaders of this virus. Rapid and effective virus detection is the one of the best solutions to stop it, without forgetting the use of vaccines to curb the spread of the epidemic [1–4].

The diagnosis of SARS-CoV-2 infection has been mainly carried out by real-time reverse transcriptase polymerase chain reaction (RT-PCR). However, this technique is expensive, requires time and qualified personnel. Hence, the development of alternative methods for the detection of the SARS-CoV-2 virus is still a great deal of interest, so recently different methods based on different techniques [5] as well as immunological tests have been developed. Biosensors are promising approaches and recently many of them based on different detection techniques [6,7], in particular electrochemical biosensors [8–12], have been reported. In this context, electrochemiluminescent (ECL) biosensors present unique properties [13–18] by combining the advantages of electrochemical and chemiluminescent biosensors and can be an excellent alternative in chemical sensing and biosensing since they offer

* Corresponding author. Grupo de Sensores Químicos y Biosensores, Departamento de Química Analítica y Análisis Instrumental, Universidad Autónoma de Madrid, 28049, Madrid, Spain.
** Corresponding author.Grupo de Sensores Químicos y Biosensores, Departamento de Química Analítica y Análisis Instrumental, Universidad Autónoma de Madrid, 28049, Madrid, Spain. .
E-mail addresses: monica.revenga@uam.es (M. Revenga-Parra), cristina.gutierrezs@uam.es (C. Gutiérrez-Sánchez).

https://doi.org/10.1016/j.talanta.2023.124614
Received 20 January 2023; Received in revised form 21 April 2023; Accepted 26 April 2023
Available online 5 May 2023

accurate determinations with high sensitivity, easy controllability, short response times, affordable cost and miniaturized instrumentation, and simple operational process [19]. In recent years, the performance of ECL biosensors has been improved with the introduction of gold nanoparticles (Au NPs). These have been used in various ways: modifying the electrode surface, enhancing surface plasmon resonance, catalyzing the reaction, improving ECL resonance energy transfer (ECL-RET), and as a nanocarrier [16]. Its properties are size and shape depending. Thus, they can be easily adjusted. This aspect is crucial in the case of ECL-RET biosensors, where they can act as efficient energy donors and acceptors. Therefore, different gold structures have been used to improve ECL-RET, due to strong localized surface plasmon resonance (LSPR) absorption. Among these structures, the most usually employed are nanoparticles [16] but other gold structures are also beginning to be used, such as nanorods [20] or nanocages [21]. These previous results confirm that high performance ECL- RET biosensors can be designed and built using gold nanostructures with shapes and sizes specially designed to tun and fully utilize their properties. Therefore, in this context one would expect that heterogeneous materials can present special relevant properties in comparison to homogeneous ones. However, few information can be found concerning the use of multilayered bimetallic core@shell nanoparticles (NPs), made of different metals, such raspberry-like bimetallic Au@Pt/Au triple-layered core@shell NPs consisting of an Au core, a Pt inner shell, and an outer shell composed of Au protuberances [22]. They consist of an Au core, a Pt inner shell, and an Au protuberances outer shell (Au@Pt/Au NPs), which allow not only to change their shape but also to increase the relative surface area. These nanostructures showed surface-enhanced Raman scattering (SERS) and electrocatalytic properties [23,24] but, to the best of our knowledge, they have not been applied in ECL system yet. Hence, in the present work we study for the first time, the use of these bifunctional core@shell Au@Pt/Au NPs as ECL signaling probes. In particular, we have employed the synthesized Au@Pt/Au NPs in a sensitive ECL-RET system combined with $[Ru(bpy)_3]^{2+}$ to develop an immunosensor for the detection of the most abundant protein of the SARS-CoV-2 coronavirus, the nucleocapsid protein (N protein). It differentiates from the spiked protein (S protein) by a mutation, has approximately 1000 copy numbers per viral particle and is highly conserved [25]. Therefore, N protein has great potential as a specific biomarker for diagnosis of COVID-19 and despite this, so far few immunosensors have been described for its detection [26,27].

2. Experimental

2.1. Chemicals and instruments

Gold (III) chloride trihydrate, silver nitrate, chloroplatinic acid solution, trisodium citrate, tris(2,2-bipyridyl) dichlororuthenium (II) hexahydrate ($[Ru(bpy)_3]^{2+}$), potassium hexacyanoferrate (III), potassium hexacyanoferrate (II) trihydrate, 98% H_2SO_4, NaOH ≥98%, bovine serum albumin (BSA), N-(3-dimethylaminopropyl)-N′-ethylcarbodiimide (EDC), N-hydroxysuccinimide (NHS), tris(hydroxymethyl) aminomethane hydrochloride (Tris-HCl) ≥99%, 2-(N-morpholino) ethanesulfonic acid (MES), potassium phosphate monobasic, sodium phosphate monobasic monohydrate ≥99%, sodium phosphate dibasic ≥99%, sodium chloride, potassium chloride, tripropylamine (TPrA) and Tween® 20 were acquired from Merck (Darmstadt, Germany). Carboxylic acid modified magnetic beads (MBs, 1 μm Ø, 10 mg/mL, Dynabeads® MyOne™ Carboxylic Acid) were obtained from Invitrogen, Fisher Scientific (Madrid, Spain).

SARS-CoV/SARS-CoV-2 Nucleoprotein capture antibody (CAb), Rabbit MAb (40,143-R004), SARS-CoV/SARS-CoV-2 Nucleoprotein detection antibody (DAb), Rabbit MAb (40,143-R040), SARSCoV-2 (2019-nCoV) Nucleocapsid His Recombinant Protein (N protein) (40,588-V08B), SARS-CoV-2 (2019-nCoV) Nucleoprotein ELISA Kit (KIT40588), Influenza A H1N1 (A/California/04/2009) Hemagglutinin/HA Protein (ECD, His Tag) (11,055-V08H), MERS-CoV Spike/S1 Protein (S1 Subunit, aa 1–725, His Tag) (40,069-V08B1) and SARS-CoV-2 (2019-nCoV) Spike S1-His Recombinant Protein (HPLC-verified) (40,591-V08H) were obtained from Sino Biological Europe GmbH (Eschborn, Germany).

Water purified obtained from a Millipore Milli-Q-System (18.2 MΩ cm at 25 °C) was used in the experiments and to prepare all solutions.

A Cary Eclipse Varian spectrofluorometer and a double beam PharmaSpec UV-1900i series spectrophotometer (Shimadzu) were used for fluorometric and spectrophotometric measurements, respectively. In both cases, spectra were recorded in aqueous solutions using a quartz cell with a 1.0 cm optical path.

Screen-printed carbon electrodes (SPCEs; ref. DRP-110; Metrohm-Dropsens) used as electrochemical cells integrate the three electrodes necessary for the measurements: carbon working and counter electrodes and a silver pseudoreference electrode.

ECL experiments were performed in an ECL cell with a potentiostat/galvanostat (±4 V DC potential range, ±40 mA maximum measurable current) and a Si-photodiode integrated from Metrohm-DropSens. To perform the measurement, it is necessary a volume of 60 μL in the ECL cell where the electrodes are confined. ECL measurements were performed using 2.0 mM $[Ru(bpy)_3]^{2+}$ in 0.1 M phosphate buffer, pH 8.0, at 0.03 V/s. In addition, ECL responses are normalized to the blank signal, which is the signal in the absence of antigen in each experiment.

Scanning electron microscopy (SEM) images were recorded in a Hitachi S-3000 N microscope with EDX analyzer Model XFlash 6I30, from Bruker.

The samples for high resolution-transmission electron microscopy (HR-TEM) were prepared using a FEI Tecnai G2 F20S-TWIN field-emission gun high resolution microscope from FEI (United States of America) on a copper grid, using an accelerating voltage of 200 kV.

Atomic Force Microscopy (AFM) images were taken on HOPG electrodes with an Agilent 5500 microscope and Olympus cantilevers (RC800PSA, 200_20 mm) operating in tapping mode in air.

2.2. Synthesis of Au@Pt/Au NPs and bioconjugation with DAb

Bifunctional core@shell Au@Pt/Au NPs were synthesized using the following methodology [24]. First, Au NPs were obtained by the Turkevich's method [28], consisting in adding 2 mL of 3.88×10^{-2} M trisodium citrate over 80 mL of 2.94×10^{-4} M gold (III) chloride trihydrate, and leaving to react during 30 min with stirring. Then, a silver shell was formed on the Au NPs by adding, over 51.25 mL of the obtained suspension (9.00×10^{14} Au NPs/mL), 3 mL of 5.88×10^{-3} M silver nitrate and 50 μL of 3.88×10^{-2} M trisodium citrate, heating to boiling and leaving to react for 1 h with stirring. After that, the silver shell was substituted by platinum through a galvanic replacement reaction, consisting in adding 80 μL of 1.95×10^{-1} M chloroplatinic acid. The obtained Au@Pt NPs were purified by centrifugation and re-suspension in water. A further silver deposition was performed adding subsequently 1.2 mL of 5.88×10^{-3} M silver nitrate and 300 μL of 3.88×10^{-2} M trisodium citrate over 45 mL of the Au@Pt NPs suspension, heating to boiling and leaving to react for 1 h with stirring. Finally, silver was replaced by Au protuberances by adding 150 μL of 2.94×10^{-4} M gold (III) chloride trihydrate and 150 μL of 3.88×10^{-2} M trisodium citrate and incubating for 20 min. The obtained Au@Pt/Au NPs suspension was finally stored at 4 °C.

Au@Pt/Au NPs were then bioconjugated with DAb (Au@Pt/Au NPs/DAb) taking advantage of the Au affinity for the thiol groups present in antibodies, adapting previously optimized protocols for other Au NPs [29] as detailed in the Supporting Information.

2.3. Modification of MBs and sandwich immunosensor

2 μL of the MBs suspension were pipetted into an Eppendorf tube and washed twice with 0.025 M MES, pH 5.0 buffer for 10 min at 25 °C under

continuous stirring (900 rpm). Between each step Eppendorf tubes were placed into a magnetic separator DynaMag™-2 (Thermo-Fisher Scientific) and, after 3 min, the supernatant was discarded. To activate the carboxylic groups of the MBs, they were incubated for 35 min with 25 μL of a freshly EDC/NHS solution (50 mg/mL each prepared in 0.025 M MES, pH 5.0 buffer) at 25 °C (900 rpm). The activated MBs were washed twice using 0.025 M MES, pH 5.0 buffer and incubated for 30 min (900 rpm) in 25 μL of a 200 ng/mL CAb in 0.025 M MES, pH 5.0 buffer. Then, the CAb-MBs were washed twice with MES, pH 5.0 buffer. Next, 25 μL of 1 mg/mL BSA in 0.1 M phosphate buffer, pH 8.0 were added to block the unreacted activated groups and therefore to prevent non-specific interactions. The mixture remained incubating for 60 min at 25 °C under continuous stirring (900 rpm). This was followed by three washes. One of them using 0.1 M Tris–HCl buffer, pH 7.2 and two with 0.01 M phosphate buffer saline, pH 7.4 by dissolving KH_2PO_4 and Na_2HPO_4 in 2.7 mM KCl and 137 mM NaCl aqueous solution including 5% (v/v) Tween® 20.

The immunoreaction with the antigen was carried out by re-suspending the CAb-MBs in 25 μL of a mixture solution containing N protein (or the sample to be analysed) and the Au@Pt/Au NPs/DAb bioconjugate and incubating for 45 min (25 °C, 900 rpm). After washing twice with 0.01 M phosphate buffer saline, pH 7.4, the MBs modified with the sandwich immunocomplex (Au@Pt/Au NPs/DAb/Nprotein/CAb-MBs) were re-suspended in 10 μL 0.1 M phosphate buffer, pH 8.0 to perform the ECL measurements.

2.4. Detection of N protein in human saliva

ECL measurements were carried out by pipetting 10 μL of the sandwich immunocomplex suspension on the working electrode surface of the SPCE, where a magnetic support was previously placed on its reverse side. After removal the excess by capillary action, the Au@Pt/Au NPs/DAb/Nprotein/CAb-MBs/SPCE was introduced into the ECL cell and 60 μL of 2.0 mM $[Ru(bpy)_3]^{2+}$ was added. The ECL signal was recorded by scanning potential from 0.0 to +1.1 V at a scan rate of 0.030 V/s.

Saliva samples were collected from healthy volunteers using a commercial Salivette® (Sarstedt) extraction kit following the specified protocol. The swab was placed in the mouth for 2 min, placed in the extraction tube and centrifuged for 2 min at 2900 rpm at 20 °C. Clear saliva samples were obtained at the conical tip of the extraction tube.

3. Results and discussion

3.1. The principle of the proposed ECL-based immunosensor

The biosensor developed is a type ECL-based sandwich immunosensor that employs for the first-time multilayered bimetallic core@shell NPs as signaling probe. The strategy followed for its development is shown in Scheme 1. First, the bifunctional core@shell Au@Pt/Au NPs made up of an Au nucleus recovered with Pt and finally decorated with small Au inlays were synthetized as previously described [24]. Initially, AuNPs were characterized by TEM (Fig. 1A). They show a spherical shape and a diameter size of 16 ± 2 nm. This diameter increases to 23 ± 3 nm for Au@Pt/Au NPs (Fig. 1B), as it is observed by HR-TEM and confirmed by AFM, that reveals a diameter of 20 nm (Fig. 1C). This increase in size distribution for the Au@Pt/AuNPs has been previously reported [24]. Additionally, Au protuberances are just observed on the surface of Au@Pt/Au NPs (Fig. 1B magnification) but not in the initial AuNPs, confirming the raspberry-like structure of the Au@Pt/Au NPs. In order to confirm the presence of both Au and Pt metals in the final Au@Pt/Au NPs, energy dispersive X-ray (EDX) analysis, associated with HR-TEM, has been performed (Fig. 1D, E and F). It is observed that the particles contain both metals, Pt and Au, with an atomic ratio of 4.37 and 95.63 ± 1.24 (n = 9) respectively, thus verifying the presence of both metals.

As depicted in Scheme 1, in the second step the specific Nucleoprotein capture antibody (CAb) is covalently immobilized on commercial magnetic beads (CAb-MBs). In parallel, Au@Pt/Au NPs are modified with the specific Nucleoprotein detection antibody (DAb) according to the described protocol in the procedures (Au@Pt/Au NPs/DAb). Once CAb-MBs and Au@Pt/Au NPs/DAb are prepared, they are incubated accompanied by Nucleocapsid His Recombinant Protein (N protein). The complete system is deposited on the surface of a SPCE and is retained on its surface using a magnet.

The biosensor principle consists of detecting the antigen-antibody recognition event by the change in the ECL signal obtained together with the luminophore $[Ru(bpy)_3]^{2+}$, using Au@Pt/Au NPs as signaling probes which act as ECL resonance energy acceptors. Several studies

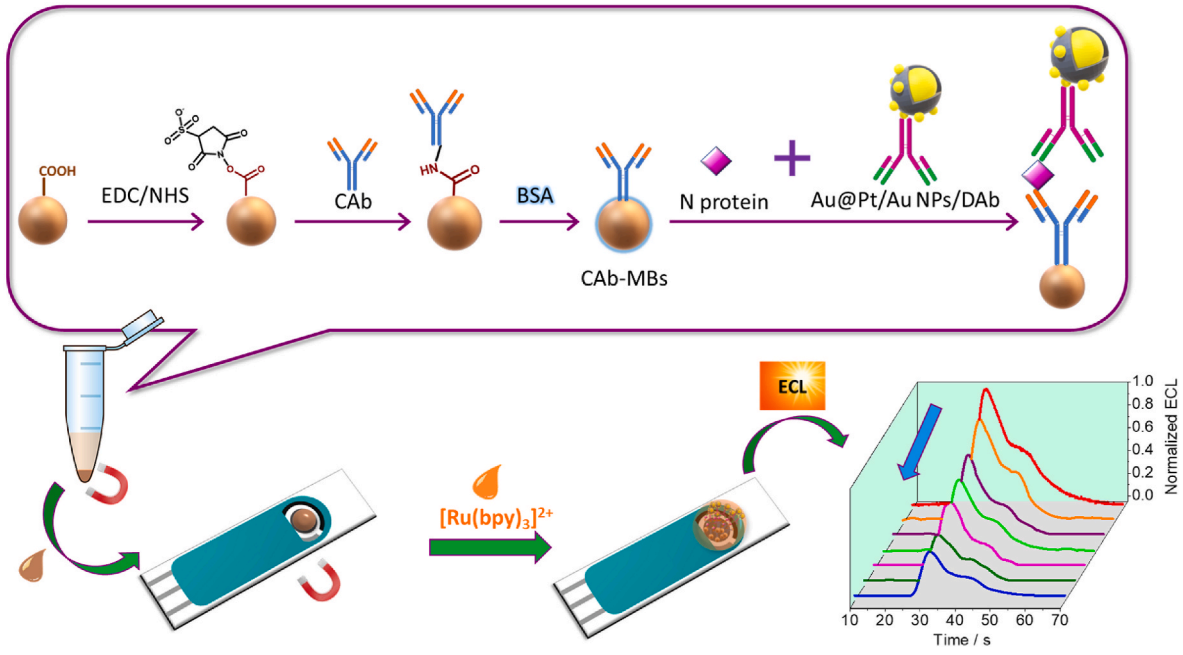

Scheme 1. Steps followed for the preparation of the immunosensor (Au@Pt/Au NPs/DAb/Nprotein/CAb-MBs/SPCE) for N protein detection.

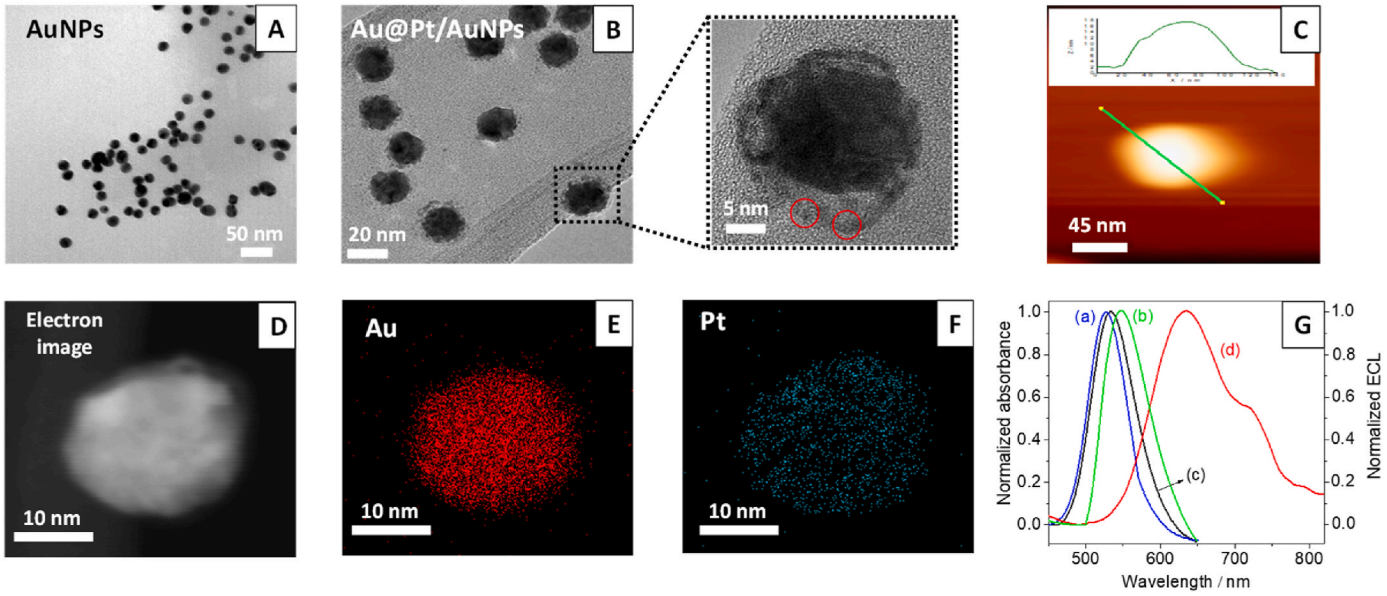

Fig. 1. (A) TEM image of Au NPs. (B) HR-TEM image of Au@Pt/Au NPs with a magnification of a single Au@Pt/Au NP. Au protuberances are labeled with a red circle. (C) AFM topographic image onto HOPG, and topographic profile across the line drawn as an inset. (D) Bright field STEM micrograph of a single nanoparticle, together with Energy dispersive X-ray (EDX) mapping of Au (E) and Pt (F). (G) Normalized UV–vis absorption spectra of 4.500×10^{14} NPs/mL of Au NPs (a), Pt–Au NPs (b) and Au@Pt/Au NPs (c). Normalized ECL emission spectrum (d) of 2.0 mM $[Ru(bpy)_3]^{2+}$ in 0.1 M phosphate buffer, pH 8.0, containing 0.25 mM TPrA obtained under a cyclic potential scan from 0.0 to +1.1 V at 0.03 V/s.

suggest [30] that the LSPR based ECL enhancement is significantly affected by the shape and size of Au@Pt/Au NPs employed.

The expected effect of shape and size of the synthetized Au@Pt/Au NPs is proved comparing the UV–vis spectrum of Au@Pt/Au NPs and the ECL emission spectrum of the $[Ru(bpy)_3]^{2+}$ in 0.25 mM TPrA. In order to better compare the degree of overlapping, both spectra have been normalized to the maximum of signal in each case. As it can be seen in Fig. 1G, there is a wide absorption band centered at 550 nm which is associated with the plasmon resonance absorption. Since the ECL emission shows a spectral band (Fig. 1G, d line) with a maximum at 620 nm and a shoulder from 700 to 750 nm, it partially overlaps with the plasmon absorption band of Au@Pt/Au NPs. Hence, the ECL response of $[Ru(bpy)_3]^{2+}$ could be significantly quenched at appropriate distance during the ECL detection process. Comparing the normalized UV–vis spectrum of Au@Pt/Au NPs with those recorded and normalized using uncompleted NPs obtained in each of the stages of their synthesis (Fig. 1G), we can observe that the UV–vis spectral bands of Pt–Au NPs are more red-shifted than Au@Pt/Au NPs. Therefore, the overlap with the ECL emission spectrum of the $[Ru(bpy)_3]^{2+}$is more pronounced and it would be expected a better efficiency of energy transfer and sensitivity of the assay. However, the shape/combination of metals of the nanostructure must play an important role also in the energy transfer since the raspberry-like nanostructure, although their spectra overlap in less extension with ECL emission spectrum of the $[Ru(bpy)_3]^{2+}$, shows the highest ECL intensity in presence of $[Ru(bpy)_3]^{2+}$ and absence of TPrA (Fig. S1). These results confirm our suppositions and justify the fact of preparing these nanoparticles as a new ECL signaling probes.

The possibility of resonance energy transfer efficiency between Au@Pt/Au NPs and $[Ru(bpy)_3]^{2+}$ is suggested by the overlap between the Au@Pt/Au NPs absorption band and the $[Ru(bpy)_3]^{2+}$ fluorescent emission band (Fig. S2).

3.2. Au@Pt/au NPs/DAb bioconjugate

We have performed different studies to demonstrate what was proposed in the main steps of the biosensor design according to Scheme 1. Hence, at a first step we have carried out studies aimed to prove the formation of the bioconjugate between the Au@Pt/Au NPs and the DAb. The mechanism of the conjugation is based on the adsorption of the antibodies, with random orientation, on the surface of the Au@Pt/Au NPs. In addition, the presence of thiol groups in the structure of the cysteine residues present in the constant region of antibodies allows this binding due to the well-known affinity of thiol groups for gold substrates.

The obtained conjugates were characterized by UV–vis absorbance spectroscopy. We studied the changes in the UV–vis spectra of Au@Pt/Au NPs in the absence and in the presence of DAb. A slight shift in λ towards the red (535 nm–543 nm) occurs when the Au@Pt/Au NPs interact with the DAb (Fig. S3A). This shift, assigned to changes in the NPs surface plasmon resonance, indicates an interaction between Au@Pt/Au NPs and DAb [24]. A decrease in absorption is also observed, which is consistent with a shielding of the plasmon band of the nanoparticles when they are covered with the antibody. The changes in the spectra of UV–vis of Au@Pt/Au NPs in presence of N protein were also studied. The absorption maximum does not undergo any displacement in this case, indicating that there is no type of specific interaction between the nanostructure and the N protein (Fig. S3B).

3.3. Characterization of the proposed ECL immunosensor

We have also performed an exhaustive morphological characterization of the different steps followed for the immunosensor development to be sure we have what we expected. This control is fundamental to fabricate reproducible devices. SEM image (Fig. 2A) shows that after the addition of the sandwich immunocomplexes suspension on the working electrode surface, it is covered by particles of nanometric size and globular shape homogeneously distributed. In the EDX-map analysis (Fig. S4), the existence of Au and Pt atoms confirms that these elements are present on Au@Pt/Au NPs. Hence, Au@Pt/Au NPs are bound to the capture antibody in the immunocomplex after N protein recognition. Fe from MBs is also evident on the EDX map. The EDX mapping of the atoms individually confirms the presence of Au@Pt/Au NPs and the magnetic beads. SEM images of the immunocomplex in absence of N protein (Fig. S5) show some areas with agglomerates of particles. However, the EDX analysis confirms the presence of Fe as expected due to the presence of the MBs (Fig. S6), but there is no evidence of Au and

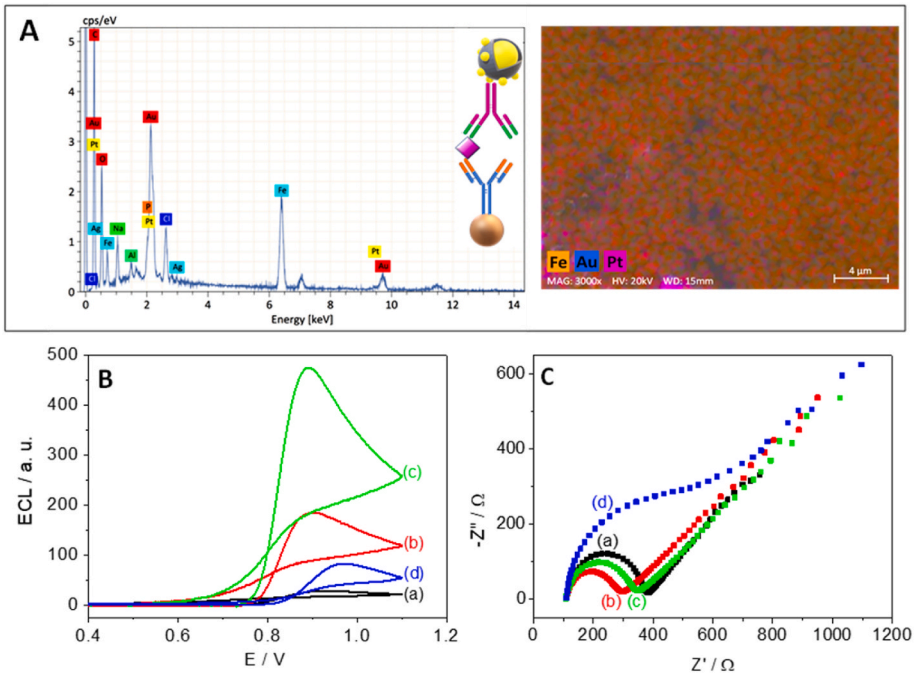

Fig. 2. (A) EDX analysis and SEM image of Au@Pt/Au NPs/DAb/Nprotein/CAb-MBs/SPCE. (B) ECL responses in presence of 2.0 mM $[Ru(bpy)_3]^{2+}$ in 0.1 M phosphate buffer, pH 8.0, at 0.03 V/s and (C) Nyquist diagrams obtained in 0.1 M phosphate buffer, pH 8.0, with 25 mM KCl in the presence of 1.0×10^{-2} mol/L $K_3Fe(CN)_6$/1.0×10^{-2} mol/L $K_4Fe(CN)_6$ for a bare SPCE (a), MBs/SPCE (b), CAb-MBs/SPCE (c), Au@Pt/Au NPs/DAb/Nprotein/CAb-MBs/SPCE (d). The N protein concentration was 20 pg/mL.

Pt. In the absence of antigen, the labeled secondary antibody does not recognize N protein and there is no trace of Au@Pt/Au NPs, which would indicate that the immunosensor has been successfully developed.

The presence of nitrogen from the antibody was not confirmed by EDX analysis since this technique does not allow its determination. Therefore, it cannot be confirmed that the globular characteristics shown in the SEM images are the antibody.

The AFM image of Au@Pt/Au NPs/DAb/Nprotein/CAb-MBs is dominated by the globular feature of the modified MBs (Fig. S7) even though the AFM tip could not define the topography of the entire molecule. The topographic profile gives a height of approximately 40 nm. The CAb-MBs conjugate has also been studied as a control. A clear difference is observed with respect to the complete immunosensing platform (Au@Pt/Au NPs/DAb/Nprotein/CAb-MBs), corroborating that the proposed system has been developed successfully.

We have also recorded the ECL signal at each immunosensor development step to perform an exhaustive control of the process (Fig. 2B). The ECL response shows a small baseline ECL signal (a), and after the addition of MBs no significant change is observed (b), while the emission of ECL increases considerably when the electrode is functionalized with Nprotein/CAb-MBs/SPCE (c), probably due to the presence of hydroxylic and amino groups present in the proteins that behave as co-reactants, which produces an increase in the ECL signal. DAb-modified Au@Pt/Au NPs (Au@Pt/Au NPs/DAb) were then introduced and acted as the signaling probe. The recognition of the N protein (Au@Pt/Au NPs/DAb/Nprotein/CAb-MBs/SPCE) produces a significant quenching in the ECL response (d) since there is an overlap of the absorption spectrum of the Au nanostructures and the emission spectrum of $[Ru(bpy)_3]^{2+}$. In our proposal, the quenching efficiency was completely related to the concentration of the target N protein what allows its detection.

In addition, the changes in the properties of the electrode surface in all the stages involved in the design of the immunosensor were studied by electrochemical impedance spectroscopy (EIS) using a 0.1 M phosphate buffer, pH 8.0 solution with 25 mM KCl and 10 mM $K_3Fe(CN)_6$/10 mM $K_4Fe(CN)_6$. Fig. 2C shows that after the deposition of the MBs onto the SPCE a decrease in the charge transfer resistance (R_{CT}) from 300 Ω (a) to 190 Ω (b) was found as a result of the high conductivity of magnetic particles. However, when the SPCE was modified with the CAb-MBs the R_{CT} increased due to the presence of the antibody (c). As can be seen in Fig. 2C (d), this increase is much more noticeable after the modification of the MBs with the sandwich immunocomplex (Au@Pt/Au NPs/DAb/Nprotein/CAb-MBs/SPCE). This behavior agrees well to the fact that the immunocomplex blocks the diffusion of the redox probe, from the solution to the electrode surface, since it forms an insulating barrier.

The immunosensor response to increasing concentrations of N protein in presence of $[Ru(bpy)_3]^{2+}$ measured at 620 nm shows it decreases as the concentration of N protein increases (Fig. S8). This behavior agrees well with the quenching of the $[Ru(bpy)_3]^{2+}$ ECL emission by the Au@Pt/Au NPs *via* ECL resonance energy transfer. Au@Pt/Au NPs effectually absorb the ECL emission of $[Ru(bpy)_3]^{2+}$ after non-radiative dissipation.

3.4. Optimization of experimental variables

Once the different steps of the immunosensor development have been characterized, the main experimental variables were optimized since they can affect the ECL response. The amount of MBs, concentration and incubation time of the CAb, concentration of Au@Pt/Au NPs, and concentration of DAb were optimized. The best response was considered when the ratio between the ECL immunosensor response in the absence (S_0) or in the presence (S) of 20 pg/mL N protein was the largest.

Optimization of the main variables, was carried out following two different strategies based on works previously published by other authors [31,32]. The first one is a single step protocol involving target protein capture and sandwiching with labeled detector antibody by means of 45 min incubation of the CAb-MBs in solution containing N protein and Au@Pt/Au NPs/DAb. The second is a two-steps strategy that involves 30 min incubation of the CAb-MBs in the N protein solution, followed by another 30 min incubation in the Au@Pt/Au NPs/DAb solution. The best response was obtained with the first one (Fig. S9). In addition, following this procedure the total assay time is reduced.

For the other experimental variables, the highest ECL signal was obtained by incubating 20 µg of MBs and 200 ng/mL of CAb for 30 min and by mixing 2.25×10^{14} NPs/mL of Au@Pt/Au NPs and 133 ng/mL of DAb to obtain the bioconjugate (Fig. 3).

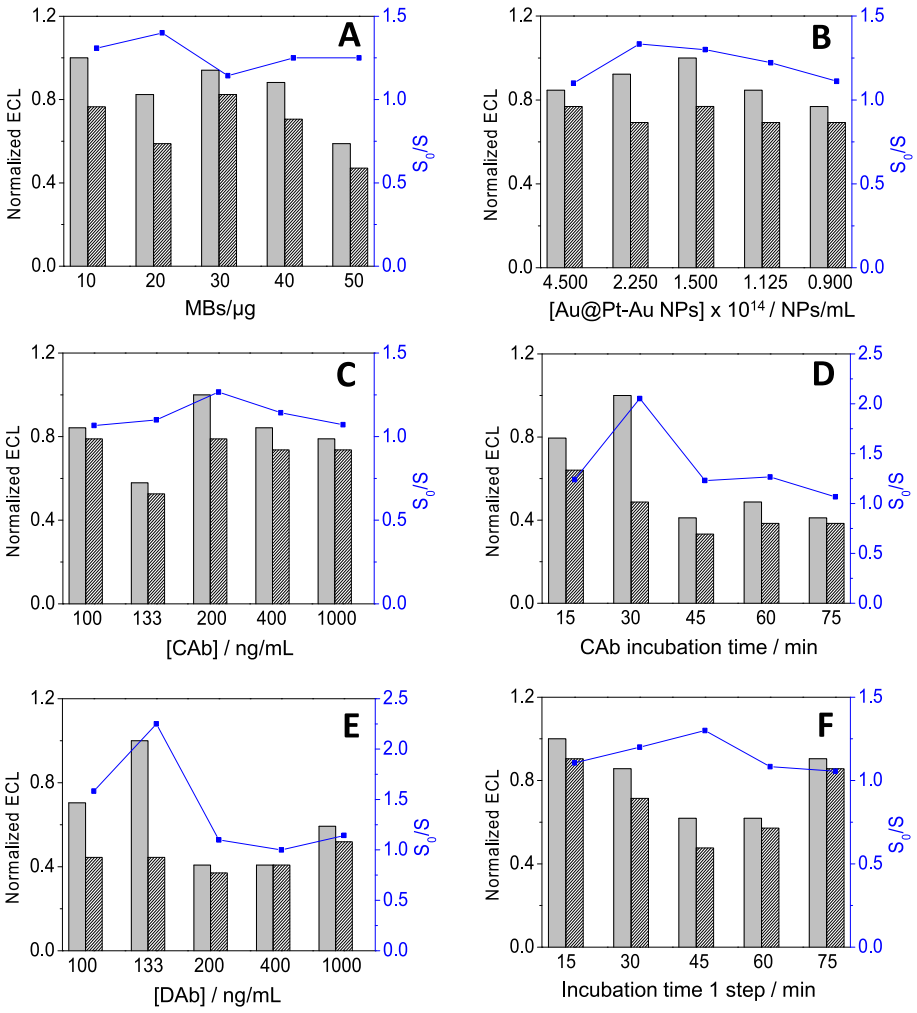

Fig. 3. Optimization of different experimental variables: (A) amount of MBs, (B) concentration of Au@Pt–Au NPs, (C) concentration of CAb, (D) incubation time of MBs with CAb, (E) concentration of DAb and (F) incubation time of CAb-MBs with the mixture of N protein and Au@Pt–Au NPs/Dab. Normalized ECL responses (left) measured in the absence (light grey bars) or in the presence (dark grey bars) of 20.0 pg/mL N protein, and the resulting S_0/S ratio (right). All the ECL responses were obtained in 0.1 M phosphate buffer, pH 8.0, in presence of 2.0 mM $[Ru\ (bpy)_3]^{2+}$.

The studies shown below were carried out with the optimized experimental variables.

3.5. Immunosensor response

The analytical properties of the final ECL immunosensor were studied. The normalized ECL response presented by the immunosensor *versus* concentration of N protein, obtained with the experimental parameters selected as optimal in the previous section, can be observed in Fig. 4. As N protein concentration increases, ECL intensity decreases.

The calibration curve shows a linear relationship between the ECL signal *versus* the standard concentration of N protein up to 240 pg/mL ($r^2 = 0.996$), which fits to the equation: ECL (a.u.) = (-24.8 ± 0.7) x10^{-2} log [N protein], pg/mL + 0.97 ± 0.01. Each point corresponds to the mean value of three determinations (Fig. 4C). The limits of detection (LD) and quantification (LQ) were calculated as three or ten times, respectively, the normalized standard deviation of the blank signal with a negative sign and the slope of the semilogarithmic curve. Value obtained has been expressed in concentration units and were found to be 1.27 pg/mL and 2.20 pg/mL, for LD and LQ, respectively. Comparing these analytical parameters with other immunosensors for the determination of N protein from SARS-CoV-2 reported (Table S1), the developed immunosensor shows one of the lowest detection limits. Hence, it has been directly applied to the detection of N protein in real samples.

The reproducibility of the ECL immunosensor was evaluated for 20.0 pg/mL N protein at five different immunosensors. The normalized ECL signals were 0.6568, 0.6679, 0.6296, 0.6740, 0.6360. From these data, the RSD was found to be 3.0%. This result confirms that the ECL immunosensor developed in this work presents good reproducibility.

A determining aspect to study for the analytical application of an immunosensor is the evaluation of the biosensor response against compounds that may interfere. Hence, the response exhibited by the immunosensor to 20.0 pg/mL N protein in the absence and presence of several proteins, such as the SARS-CoV-2 Spike S1-His recombinant protein, the MERS-CoV Spike S1 protein and the influenza A H1N1 Hemagglutinin was evaluated. In the presence of each potential interfering protein studied, no significant changes in ECL response (Fig. 4D) were found, confirming the selectivity of the designed immunosensor. The results indicate that the immunosensor allows to determine the N protein in a highly selective manner, being able to discriminate between the S protein and N protein.

The stability of the immunosensor response was evaluated for 700 s by applying consecutive cycles of potential sweep between 0.0 V and +1.1 V in a 2.0 mM $[Ru\ (bpy)_3]^{2+}$ in 0.1 M phosphate buffer, pH 8.0 (Fig. 4E). The ECL signal remained stable during the time studied, maintaining 97% of the initial value. Also, the storage stability of the immunosensor was studied. A loss of 2.6% of the initial ECL response was observed after storage of the immunosensing platform at 4 °C in a humid chamber for 45 days (Fig. 4F). Therefore, the developed immunosensor presents high stability.

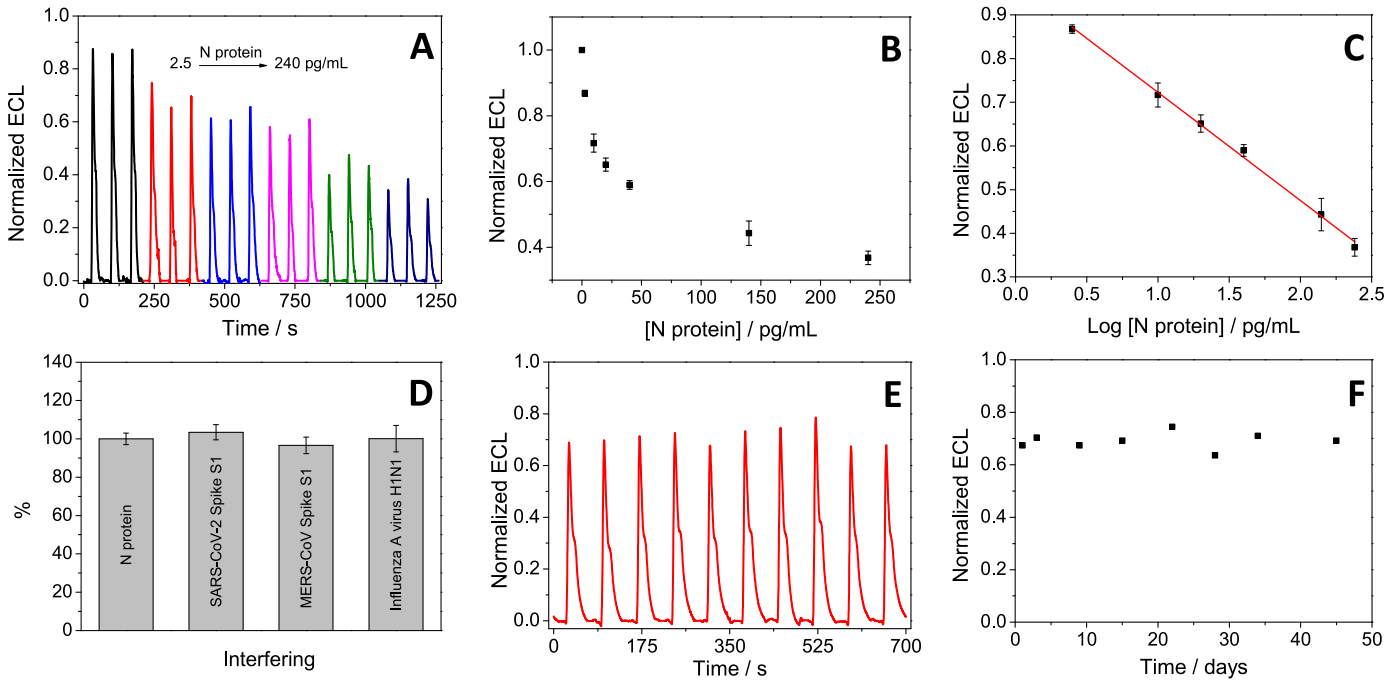

Fig. 4. (A) Normalized ECL immunosensor response to various concentrations N protein. (B) Calibration curve of normalized ECL intensity *vs* N protein concentrations (n = 3). (C) Linear plot of the normalized ECL intensity *vs* logarithmic concentration of N protein (n = 3). (D) Immunosensor response (n = 3) to 20.0 pg/mL N protein obtained in the absence and in presence of 20.0 pg/mL different potential interfering proteins. (E) ECL signal-time curve of 20.0 pg/mL N protein obtained under continuous cycles. (F) Storage stability of the immunosensor measured for 45 days. All measurements were carried out in 0.1 M phosphate buffer, pH 8.0 aqueous solution containing 2.0 mM $[Ru(bpy)_3]^{2+}$.

3.6. N protein determination in human saliva

The ECL-based immunosensor was used for the determination of N protein in human saliva samples. The treatment of the samples is described in the procedures section. The un-normalized ECL signal is shown in Fig. S10. The values obtained for N protein and the recovery achieved, from the analysis carried out in triplicate are shown in Table 1. The recoveries obtained at different levels of N protein concentration were 103%–104%. A standard sandwich ELISA kit was used to compare and validate the results obtained. As shown in Table 1, unlike the developed immunosensor, the ELISA kit was not able to detect N protein concentrations equal to or less than 50 pg/mL, indicating that the sensitivity of the ECL immunosensor is better than that of the commercial kit. In addition, when comparing the values obtained by both methods for higher concentrations, it is observed that the average concentration value for 200 pg/mL of N protein agree with those obtained with the ELISA kit. These results demonstrate that the ECL-based immunosensor can be utilized for the determination of N protein from the SARS-CoV-2 in human saliva.

Table 1
Values obtained for the determination of N protein from SARS-CoV-2 with the immunosensor developed based on ECL and with a comparative colorimetric method such as the ELISA kit, in saliva samples (n = 3).

Saliva Sample	Immunosensor			ELISA		
	N protein Added (pg/mL)	N protein Found (pg/mL)	Recovery (%)	N protein Added (pg/mL)	N protein Found (pg/mL)	Recovery (%)
Sample 1	0	n. d.	-	0	n. d.	-
	2.5	2.6 ± 0.1	103	2.5	n. d.	-
Sample 2	0	n. d.	-	0	n. d.	-
	50	52 ± 3	104	50	n. d.	-
Sample 3	0	n. d.	-	0	n. d.	-
	200	209 ± 7	104	200	219 ± 3	110

4. Conclusions

Due to the pandemic that we have suffered caused by the SARS-CoV-2 coronavirus, the design of biosensors, as rapid and affordable method for diagnosis and therefore as a useful tool to contain the spread of the disease, has been a deal of great interest. We have developed a new immunosensor based on electrochemiluminescent resonance energy transfer (ECL-RET) for the rapid detection of N protein from the SARS-CoV-2 coronavirus in a highly selective manner, using $[Ru(bpy)_3]^{2+}$ as an ECL donor and bifunctional core@shell Au@Pt/Au NPs as an ECL acceptor.

Au@Pt/Au NPs, used as a signaling probes, are nanoparticles that are made up of an Au core, then coated with Pt, and finally decorated with small Au inlays. The use of these nanoparticles has turned out to be fundamental for the development of this immunosensor since they act as signaling probes in the ECL response.

The developed immunosensor showed a detection limit of 1.27 pg/mL and a broad linear response with an RSD of 3%. In addition, the immunosensor directly determined the N protein in human saliva samples.

Ease of use combined with non-invasive sampling give this ECL-based immunosensor high potential for the detection of SARS-CoV-2 in saliva with high sensitivity.

Declaration of competing interest

The authors declare that they have no known competing financial interests or personal relationships that could have appeared to influence the work reported in this paper.

Data availability

Data will be made available on request.

Acknowledgments

The authors wish to express their sincere thanks to the Spanish Ministerio de Ciencia e Innovacion (MICINN) (PID2020-116728RB-I00 and PID2020-115204RB-I00) and the Comunidad Autónoma de Madrid (S2018/NMT-4349 TRANSNANOAVANSENS-CM Program, SI3/PJI/2021–00341 and 2021-5A/BIO-20943 Talent Attraction Project) for the financial support. C. Toyos-Rodríguez acknowledges the MICINN for the award of a FPI Grant (PRE2018-084953). A. de la Escosura-Muñiz also thanks the MICINN for the research founding by a "Ramón y Cajal" contract (RyC-2016-20299).

Appendix A. Supplementary data

Supplementary data to this article can be found online at https://doi.org/10.1016/j.talanta.2023.124614.

References

[1] A. Parihar, P. Ranjan, S.K. Sanghi, A.K. Srivastava, R. Khan, Point-of-Care biosensor-based diagnosis of COVID-19 holds promise to combat current and future pandemics, ACS Appl. Bio Mater. 3 (2020) 7326–7343.
[2] T. Pinheiro, A.R. Cardoso, C.E.A. Sousa, A.C. Marques, A.P.M. Tavares, A.M. Matos, et al., Paper-based biosensors for COVID-19: a review of innovative tools for controlling the pandemic, ACS Omega 6 (2021) 29268–29290.
[3] E. Morales-Narváez, C. Dincer, The impact of biosensing in a pandemic outbreak: COVID-19, Biosens. Bioelectron. 163 (2020), 112274.
[4] F. Mollarasouli, N. Zare-Shehneh, M. Ghaedi, A review on corona virus disease 2019 (COVID-19): current progress, clinical features and bioanalytical diagnostic methods, Microchim. Acta 189 (2022) 103.
[5] C.H. Woo, S. Jang, G. Shin, G.Y. Jung, J.W. Lee, Sensitive fluorescence detection of SARS-CoV-2 RNA in clinical samples via one-pot isothermal ligation and transcription, Nature Biomedical Engineering 4 (2020) 1168–1179.
[6] H. Maddali, C.E. Miles, J. Kohn, D.M. O'Carroll, Optical biosensors for virus detection: prospects for SARS-CoV-2/COVID-19, Chembiochem 22 (2021) 1176–1189.
[7] N. Bhalla, A.F. Payam, A. Morelli, P.K. Sharma, R. Johnson, A. Thomson, et al., Nanoplasmonic biosensor for rapid detection of multiple viral variants in human serum, Sensor. Actuator. B Chem. 365 (2022), 131906.
[8] A. Raziq, A. Kidakova, R. Boroznjak, J. Reut, A. Öpik, V. Syritski, Development of a portable MIP-based electrochemical sensor for detection of SARS-CoV-2 antigen, Biosens. Bioelectron. 178 (2021), 113029.
[9] A. Erdem, H. Senturk, E. Yildiz, M. Maral, Amperometric immunosensor developed for sensitive detection of SARS-CoV-2 spike S1 protein in combined with portable device, Talanta 244 (2022), 123422.
[10] W.-I. Lee, A. Subramanian, S. Mueller, K. Levon, C.-Y. Nam, M.H. Rafailovich, Potentiometric biosensors based on molecular-imprinted self-assembled monolayer films for rapid detection of influenza A virus and SARS-CoV-2 spike protein, ACS Appl. Nano Mater. 5 (2022) 5045–5055.
[11] C. Jiang, X. Mu, B. Du, Z. Tong, A review of electrochemical biosensor application in the detection of the SARS-COV-2, Micro & Nano Lett. 17 (2022) 49–58.
[12] C.-C. Wu, Y.-H. Chiang, H.-Y. Chiang, A label-free electrochemical impedimetric immunosensor with biotinylated-antibody for SARS-CoV-2 Nucleoprotein detection in saliva, Biosensors 12 (2022) 265.
[13] Y. Chen, S. Zhou, L. Li, J.-j. Zhu, Nanomaterials-based sensitive electrochemiluminescence biosensing, Nano Today 12 (2017) 98–115.
[14] P. Bertoncello, R.J. Forster, Nanostructured materials for electrochemiluminescence (ECL)-based detection methods: recent advances and future perspectives, Biosens. Bioelectron. 24 (2009) 3191–3200.
[15] S. Deng, H. Ju, Electrogenerated chemiluminescence of nanomaterials for bioanalysis, Analyst 138 (2013) 43–61.
[16] T.T. Bezuneh, T.H. Fereja, S.A. Kitte, H. Li, Y. Jin, Gold nanoparticle-based signal amplified electrochemiluminescence for biosensing applications, Talanta 248 (2022), 123611.
[17] T. Guerrero-Esteban, C. Gutiérrez-Sánchez, E. Martínez-Periñán, M. Revenga-Parra, F. Pariente, E. Lorenzo, Sensitive glyphosate electrochemiluminescence immunosensor based on electrografted carbon nanodots, Sensor. Actuator. B Chem. 330 (2021), 129389.
[18] T. Guerrero-Esteban, C. Gutiérrez-Sánchez, A.M. Villa-Manso, M. Revenga-Parra, F. Pariente, E. Lorenzo, Sensitive SARS-CoV-2 detection in wastewaters using a carbon nanodot-amplified electrochemiluminescence immunosensor, Talanta 247 (2022), 123543.
[19] Y.-Y. Zhang, Q.-M. Feng, J.-J. Xu, H.-Y. Chen, Silver nanoclusters for high-efficiency quenching of CdS nanocrystal electrochemiluminescence and sensitive detection of microRNA, ACS Appl. Mater. Interfaces 7 (2015) 26307–26314.
[20] M. Wu, Z. Chen, H. Xu, A. Zhang, Sensitive electrochemiluminescence resonance energy transfer (ECL-RET) between Ru(bpy)32+and Au nanorod for hydrogen peroxide detection, Sci. China Chem. 60 (2017) 410–414.
[21] H.-J. Lu, J.-B. Pan, Y.-Z. Wang, S.-Y. Ji, W. Zhao, X.-L. Luo, et al., Electrochemiluminescence energy resonance transfer system between RuSi nanoparticles and hollow Au nanocages for nucleic acid detection, Anal. Chem. 90 (2018) 10434–10441.
[22] W. Xie, C. Herrmann, K. Kömpe, M. Haase, S. Schlücker, Synthesis of bifunctional Au/Pt/Au core/shell nanoraspberries for in situ SERS monitoring of platinum-catalyzed reactions, J. Am. Chem. Soc. 133 (2011) 19302–19305.
[23] X.-R. Li, M.-C. Xu, H.-Y. Chen, J.-J. Xu, Bimetallic Au@Pt@Au core–shell nanoparticles on graphene oxide nanosheets for high-performance H2O2 bi-directional sensing, J. Mater. Chem. B 3 (2015) 4355–4362.
[24] A. Iglesias-Mayor, O. Amor-Gutiérrez, A. Novelli, M.-T. Fernández-Sánchez, A. Costa-García, A. de la Escosura-Muñiz, Bifunctional Au@Pt/Au core@shell nanoparticles as novel electrocatalytic tags in immunosensing: application for alzheimer's disease biomarker detection, Anal. Chem. 92 (2020) 7209–7217.
[25] J. Ou, Z. Zhou, R. Dai, J. Zhang, S. Zhao, X. Wu, et al., V367F mutation in SARS-CoV-2 spike RBD emerging during the early transmission phase enhances viral infectivity through increased human ACE2 receptor binding affinity, J. Virol. 95 (2021) e00617–e00621.
[26] Y. Chen, Y. He, J. Zhao, J. Zhang, R. Yuan, S. Chen, Hydrophobic localized enrichment of Co-reactants to enhance electrochemiluminescence of conjugated polymers for detecting SARS-CoV-2 nucleocapsid proteins, Anal. Chem. 94 (2022) 4446–4454.
[27] Y. Wen, G. Yang, J. Zhao, Y. He, R. Yuan, S. Chen, An electrochemiluminescence biosensor based on morphology controlled iridium complex nanomaterials for SARS-CoV-2 nucleocapsid protein detection, Sensor. Actuator. B Chem. 371 (2022), 132602.
[28] J. Turkevich, P.C. Stevenson, J. Hillier, A study of the nucleation and growth processes in the synthesis of colloidal gold, Discuss. Faraday Soc. 11 (1951) 55–75.
[29] A. Ambrosi, M.T. Castañeda, A.J. Killard, M.R. Smyth, S. Alegret, A. Merkoçi, Double-codified gold nanolabels for enhanced immunoanalysis, Anal. Chem. 79 (2007) 5232–5240.
[30] S.J. Barrow, A.M. Funston, D.E. Gómez, T.J. Davis, P. Mulvaney, Surface plasmon resonances in strongly coupled gold nanosphere chains from monomer to hexamer, Nano Lett. 11 (2011) 4180–4187.
[31] C. Kacar, R.M. Torrente-Rodriguez, M. Pedrero, S. Campuzano, E. Kilic, J. M. Pingarron, Amperometric magnetoimmunoassay for the determination of lipoprotein(a), Microchim. Acta 182 (2015) 1457–1464.
[32] R.M. Torrente-Rodriguez, S. Campuzano, V. Ruiz-Valdepenas-Montiel, M. Pedrero, M.J. Fernandez-Acenero, R. Barderas, et al., Rapid endoglin determination in serum samples using an amperometric magneto-actuated disposable immunosensing platform, J. Pharmaceut. Biomed. Anal. 129 (2016) 288–293.